International Journal of Nanomedicine

Dovepress
Taylor & Francis Group

Open Access Full Text Article

ORIGINAL RESEARCH

A Thermosensitive Hydrogel Embedded with Metronidazole-Derived Carbon Dots for Antibacterial Treatment of Periodontitis

Dingjie Wang[1,2,*], Xingrong Feng[1,2,*], Xiaoyi Tang[3], Yuntong Hu[1,2], Xiaodong Xing[4], Yuhong Xiao[1,2]

[1]Yunnan Key Laboratory of Stomatology, Department of Dental Research, Kunming Medical University, Kunming, People's Republic of China; [2]Department of Oral Surgery, 920th Hospital of Joint Logistics Support Force of PLA, Kunming Medical University, Kunming, People's Republic of China; [3]Department of Stomatology, The First People's Hospital of Yunnan Province, Kunming, People's Republic of China; [4]College of Chemical Engineering, Nanjing University of Science and Technology, Nanjing, People's Republic of China

*These authors contributed equally to this work

Correspondence: Yuhong Xiao, Department of Oral Surgery, 920th Hospital of Joint Logistics Support Force of PLA, Kunming Medical University, Kunming, People's Republic of China, Email xiaoyuhong56@126.com; Xiaodong Xing, College of Chemical Engineering, Nanjing University of Science and Technology, Nanjing, People's Republic of China, Email xingxiaodong07@njust.edu.cn

Introduction: Microorganisms are the primary initiators of periodontitis, and local antibiotic therapy remains an important adjunctive strategy for controlling periodontal pathogenic bacteria. However, conventional antimicrobial agents often exhibit limited local retention and may induce cytotoxicity or bacterial resistance. This study aimed to develop a thermosensitive hydrogel system incorporating metronidazole-derived carbon dots (Met-CDs) for localized antibacterial treatment of periodontitis.

Methods: Met-CDs were synthesized via a one-step hydrothermal method at different temperatures, and their physicochemical characteristics were compared. Human gingival fibroblasts (HGFs) were used to evaluate cytocompatibility through CCK-8 and live/dead staining assays. Antibacterial activity of Met-CDs against Streptococcus sanguinis, Porphyromonas gingivalis, and Fusobacterium nucleatum was assessed using metabolic activity assays, live/dead bacterial staining, scanning electron microscopy, and Western blot analysis. A Poloxamer 407 (P407)-based thermosensitive hydrogel was further fabricated and characterized by rheological, swelling, and in vitro release analyses, while its antibacterial activity was evaluated using agar well antibacterial assays. In vivo biosafety was evaluated in an SD rat model through hematological analysis, inflammatory cytokine ELISA, and histological staining, while therapeutic efficacy was assessed by bacterial load analysis, immunohistochemical analysis, and micro-CT assessment.

Results: Met-CDs synthesized at 180 °C retained relatively enriched polar and oxidized surface groups compared with those synthesized at 250 °C, which was associated with enhanced antibacterial activity, and were therefore selected for subsequent studies. Compared with metronidazole (Met), Met-CDs demonstrated enhanced antibacterial activity and lower cytotoxicity toward HGFs. Western blot analysis suggested that the antibacterial effect of Met-CDs may be associated with bacterial membrane disruption. The Met-CDs@P407 hydrogel exhibited favorable thermosensitive behavior, swelling properties, in vitro release characteristics, and retained in vitro antibacterial activity. In vivo experiments demonstrated acceptable biosafety of the hydrogel system, with no obvious systemic inflammatory response or organ toxicity observed under the tested conditions. In addition, the hydrogel reduced periodontal bacterial burden and alleviated alveolar bone resorption in SD rats with experimental periodontitis. Although immunohistochemical staining revealed no obvious enhancement of VEGF expression, indicating a limited effect on VEGF-mediated angiogenic activity, decreased TNF-α expression was observed in periodontal tissues, suggesting that Met-CDs@P407 may alleviate local inflammatory responses through effective control of periodontal pathogenic bacteria.

Conclusion: The Met-CDs@P407 thermosensitive hydrogel demonstrated favorable antibacterial activity, cytocompatibility, localized retention potential, and in vivo therapeutic efficacy, suggesting its potential as a localized antimicrobial biomaterial for periodontitis treatment.

https://doi.org/10.2147/IJN.S604753
Received: 23 February 2026
Accepted: 22 May 2026
Published: 27 May 2026

Plain Language Summary:

1. Metronidazole-derived carbon dots synthesized at 180 °C retain richer surface functionalities.
2. Metronidazole-derived carbon dots exhibit lower cytotoxicity than metronidazole.
3. The metronidazole-derived carbon dot-embedded thermosensitive hydrogel demonstrates effective localized antibacterial activity against periodontal pathogens.

Keywords: carbon dots, metronidazole, thermosensitive hydrogel, periodontitis

Introduction

Microorganisms are the primary initiators of periodontitis, which subsequently leads to periodontal tissue attachment loss mediated by the host immune response.[1,2] The prevalence of periodontitis is high and continues to rise globally. Between 2020 and 2022, the worldwide prevalence of periodontitis reached 62%, with severe periodontitis accounting for as much as 23.6%.[3] Current clinical strategies rely primarily on mechanical therapy supplemented with antibiotics.[4] Metronidazole has long been used as an adjunctive agent in the treatment of periodontitis and is widely prescribed in cases of severe periodontal infection due to its potent activity against anaerobic bacteria.[5,6] However, systemic antibiotic administration often results in suboptimal local drug concentrations and contributes to bacterial resistance.[7,8] Furthermore, local gel-based treatments still face operational challenges, as drugs injected into periodontal pockets struggle to remain in place, ultimately compromising their therapeutic efficacy.[9,10] To address these limitations, thermosensitive hydrogel-based local delivery systems have attracted increasing attention due to their ability to undergo sol–gel transition at physiological temperature, thereby enhancing drug retention at the target site. Previous studies have demonstrated progress in optimizing drug delivery through improved mechanical properties and sustained release profiles.[11] However, further improvements in antibacterial efficacy remain challenging while maintaining effective local retention and favorable handling properties. Therefore, there is a need to develop biomaterials that integrate potent localized antibacterial activity, low toxicity, and good clinical operability.

In recent years, carbon dots (CDs), a novel class of zero-dimensional carbon nanomaterials with excellent biocompatibility, have emerged as promising solutions for addressing bacterial resistance and effectively eliminating bacterial biofilms.[12–14] CDs synthesized from different carbon sources exhibit distinct biological properties and generally possess broad-spectrum antibacterial activity against both Gram-positive and Gram-negative bacteria.[15] The three primary antibacterial mechanisms reported for CDs include physical and mechanical disruption of bacterial membranes, generation of reactive oxygen species (ROS), and damage to bacterial DNA and proteins.[16] Additionally, CDs are ultrasmall in size (<10 nm) and contain multiple surface functional groups, allowing them to interact readily with both inorganic and organic molecules. As a result, CDs can be rapidly internalized by cells, making them ideal candidates for drug delivery systems in both animal and human therapeutic applications.[17]

Based on this rationale, we envisioned that embedding metronidazole-derived carbon dots (Met-CDs) into a Poloxamer 407 (P407)-based thermosensitive hydrogel would simultaneously enhance localized antibacterial efficacy and improve drug retention within periodontal pockets. Compared with previously reported thermosensitive hydrogel systems that primarily focus on sustained drug release, the present design aims to introduce functional nanomaterials to further improve antibacterial performance while preserving the advantages of thermosensitive gelation. We further postulated that Met-CDs would exhibit superior antibacterial activity compared to metronidazole at equivalent concentrations, as verified through a series of in vitro antibacterial assays. In addition, the sol–gel transition behavior of the hydrogel at body temperature was expected to facilitate prolonged retention at the application site, thereby enhancing the localized antibacterial effect. These hypotheses were subsequently partially validated in a rat model of experimental periodontitis. The synthetic strategy and functional validation of the hydrogel system are illustrated in Figure 1.

Materials and Methods

Selection and Characterization of the Met-CDs Preparation Methods

On the basis of previous reports, the Met-CDs were synthesized via a hydrothermal method.[18] Briefly, 99% metronidazole (Aladdin, Shanghai, China) was dissolved in 10 mL of deionized water and ultrasonicated. The solution was

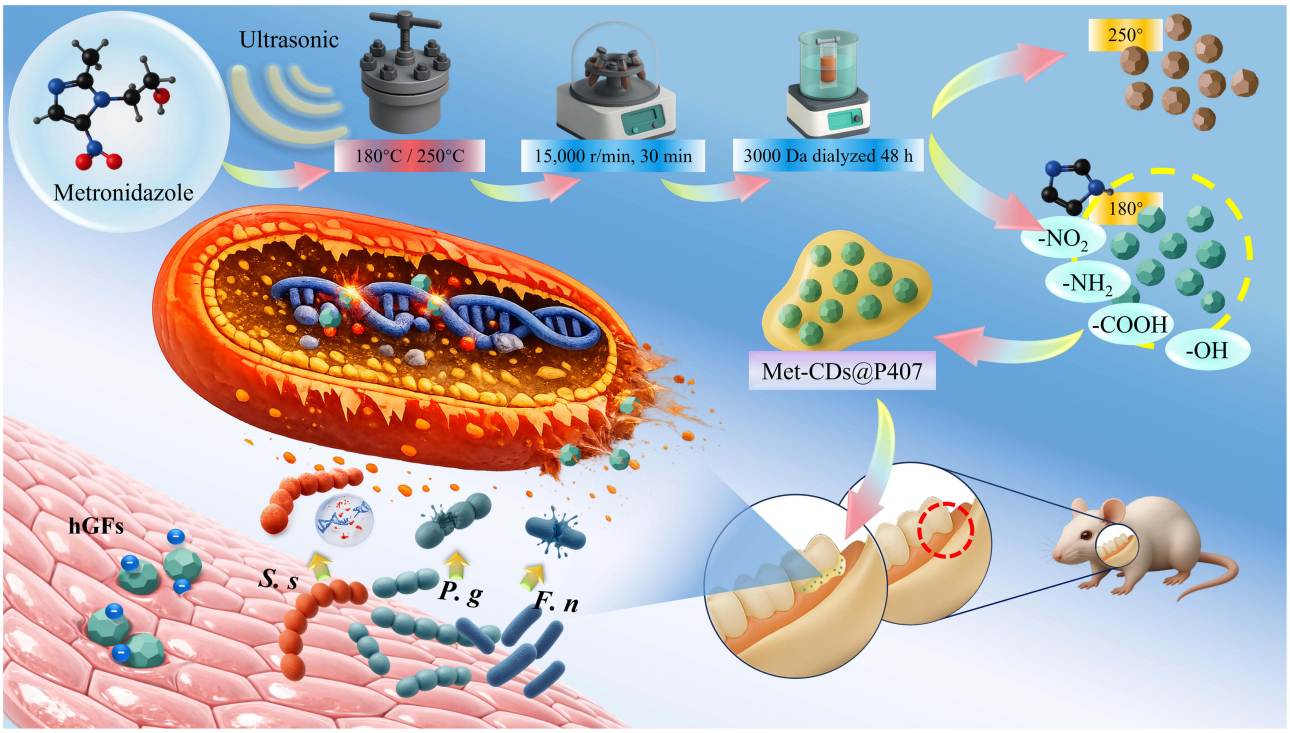

Figure 1 Synthesis of metronidazole carbon dots (Met-CDs) and their incorporation into a thermosensitive hydrogel. The Met-CDs exhibited good biocompatibility with human gingival fibroblasts and potent antibacterial activity against *Streptococcus sanguinis* (S.s), *Fusobacterium nucleatum* (F.n), and *Porphyromonas gingivalis* (P.g). The Met-CDs @P407 also effectively inhibited disease progression in a Sprague–Dawley (SD) rat model of experimental periodontitis. The yellow dotted circle indicates the newly synthesized Met-CDs prepared at 180 °C selected in this study, while the red dotted circle indicates the first molar region where the experimental periodontitis model was established in SD rats.

transferred to a muffle furnace, heated to 180°C or 250°C within 30 min, maintained for 8 h, and then naturally cooled. The resulting brown turbid suspension was centrifuged at 15,000 r/min for 30 min, and the supernatant was dialyzed against a 3000 Da membrane for 48 h. The obtained Met-CDs solution was freeze-dried into a powder and stored at 4°C.

Characterization of the Met-CDs was performed via Fourier transform infrared spectroscopy (FTIR) (Nicolet iS10, Thermo Fisher Scientific, USA) for functional group analysis, UV–Vis spectroscopy (Biomate 3S, Thermo Fisher Scientific, USA) for absorption spectroscopy (200–1000 nm), and X-ray photoelectron spectroscopy (XPS) (Krados, UK) with Al Kα (1486.6 eV) as the X-ray excitation source. High-resolution transmission electron microscopy (HRTEM) (JEM-2010, Thermo Fisher Scientific, USA) at an acceleration voltage of 200 kV was used to capture images, and the particle size distribution was analyzed via Nano Measurer software. The zeta potential of the Met-CDs was measured via a zeta potential analyzer (Nano ZS90, Malvern Panalytical, UK). The optimal preparation method was selected on the basis of the characterization results of subsequent experiments.

CCK-8 Cytotoxicity Assay

The cytotoxicity of Met, Met-CDs and Met-CDs@P407 at different concentrations was evaluated in human gingival fibroblasts (HGFs) (CP-H240, Procell, China). Cells between passages 3 and 6 were used for all experiments. For Met and Met-CDs groups, cells were seeded in 96-well plates and incubated for 24 h. Subsequently, 200 μL of Met or Met-CDs solutions at different concentrations were added to each well, with untreated cells serving as negative controls. For the Met-CDs@P407 group, hydrogels at corresponding concentrations were first placed at the bottom of the wells, followed by seeding of HGFs onto the hydrogel-containing wells and incubation for 24 h. After treatment, 100 μL of fresh serum-free DMEM and 10 μL of CCK-8 reagent (BS350B, Biosharp, China) were added to each well, followed by a 2 h incubation in the dark. The absorbance was measured at 450 nm via a microplate reader (ELX800, Biotek, USA). The experiment was repeated three times, and the relative cell viability was calculated.

https://doi.org/10.2147/IJN.S604753

Live/Dead Cell Fluorescence Staining

A live/dead cell fluorescence staining kit (CA1630, Solarbio, China) was used to evaluate the effects of Met, Met-CDs and the Met-CDs@P407 on HGFs viability. The cells were seeded on coverslips in 24-well plates and incubated for 24 h. The control group contained only the culture medium, whereas the experimental groups were treated with different concentrations of the Met and Met-CDs solutions for 24 h. After staining, fluorescence microscopy was used to observe cell viability.

Antibacterial Activity Assay

The antibacterial activity of the Met-CDs was tested against major periodontal pathogens, including *Porphyromonas gingivalis* (*P. gingivalis*, ATCC33277), *Fusobacterium nucleatum* (*F. nucleatum*, ATCC25586), and *Streptococcus sanguinis* (*S. sanguinis*, ATCC10556). All bacterial strains were obtained from the American Type Culture Collection (ATCC) and adjusted to a concentration of 1×10^6 CFU/mL.

The minimum inhibitory concentration (MIC) of the Met-CDs was determined via the turbidity method. Serial twofold dilutions of the Met and Met-CD solutions were prepared and mixed with 10 μL of bacterial suspensions (1×10^6 CFU/mL). The blank control contained only brain–heart infusion (BHI) medium, whereas the positive control consisted of bacteria cultured in BHI medium. The samples were incubated anaerobically at 37°C for 24 h, and the MIC was determined via visual inspection of the first transparent tube. The minimum bactericidal concentration (MBC) was determined by streaking the MIC sample onto BHI agar plates, incubating it anaerobically at 37°C for 24 h, and identifying the lowest concentration with no visible bacterial growth. Each experiment was performed in triplicate.

Bacterial Metabolic Activity Assay

Met and Met-CDs solutions were prepared at various concentrations. In 96-well microplates, 200 μL of each solution was mixed with 10 μL of bacterial suspensions (1×10^6 CFU/mL) and incubated anaerobically at 37°C for 24 h. After incubation, 20 μL of CCK-8 reagent was added to each well, and the samples were incubated in the dark for 2 h. The absorbance was measured at 450 nm via a microplate reader. Higher absorbance values indicated greater metabolic activity in live bacteria. Each concentration was tested in five replicates, and the experiment was performed three times.

Live/Dead Bacterial Staining Assay

Bacteria were treated with different concentrations of Met and Met-CDs, with sterile BHI medium serving as the blank control. After anaerobic incubation at 37°C for 24 h, the bacterial suspensions were collected and stained via the LIVE/DEAD bacterial viability kit (LIVE/DEAD BacLight, L7012, Molecular Probes, USA). A confocal laser scanning microscope (CLSM, LSM 800, Germany) was used to observe fluorescence staining, where live bacteria appeared green (stained with SYTO9) and dead bacteria with compromised membranes appeared red (stained with propidium iodide).

Bacterial Biofilm Observation

Following approval from the Ethics Committee of the 920 Hospital of the Joint Logistics Support Force of the Chinese People's Liberation Army (2023–024-01), fresh caries-free third molars were collected and sectioned into dentin discs (0.5 × 0.5×0.1 cm). The discs were sterilized by autoclaving.

Dentin discs were immersed in bacterial suspensions and incubated with the drug solutions for 24 h to allow biofilm formation. The MIC/MBC concentrations of the Met-CDs were selected, and the Met group was treated only at the same concentration as the MBC of the Met-CDs. The biofilm-covered dentin was gently rinsed with sterile PBS to remove planktonic bacteria, fixed with 2.5% glutaraldehyde for 24 h, dehydrated in a graded ethanol series (30%, 50%, 70%, 85%, 95%, and 100%), freeze-dried, sputter-coated with gold, and observed by scanning electron microscopy (SEM5000, China).

Western Blot Analysis of Bacterial Cytoplasmic Protein Leakage

To assess membrane and cell wall damage induced by the materials, Western blot analysis was performed to quantify cytoplasmic protein leakage from bacterial cells. Suspensions of *P. g., F.* n., and *S. s*. were adjusted to a concentration of 1×10^6 CFU/mL. Three groups were established for each species: (1) blank control, (2) metronidazole (Met), and (3) metronidazole-derived carbon dots (Met-CDs), with three independent replicates per group (n = 3). The Met and Met-CDs groups were treated at the minimum bactericidal concentration (MBC) determined for Met-CDs against each species, enabling a direct comparison of antibacterial efficacy at equivalent concentrations. After 2 h of anaerobic incubation, bacterial suspensions were centrifuged at 8000 × g for 20 min at 4 °C. The resulting cell pellets were collected for protein extraction.

GroEL, a highly conserved intracellular chaperonin that plays a critical role in protein folding and cellular homeostasis, was selected as the target marker to evaluate cytoplasmic protein retention and membrane integrity.[19] Equal loading of samples was ensured by normalizing the pellet amount in each group using Ponceau S staining prior to electrophoresis. After SDS-PAGE and transfer to PVDF membranes, membranes were blocked and then incubated with a primary antibody against GroEL (EPR28718-8, Abcam, UK) (dilution ratio: 1:1000), followed by HRP-conjugated secondary antibodies. Immunoreactive bands were visualized using chemiluminescence and quantified by densitometry analysis (eg., using ImageJ software). Variations in GroEL levels among groups served as an indirect indicator of membrane and wall integrity disruption.

Preparation of the Thermosensitive Hydrogel with Met-CDs

Poloxamer 407 (9003–11-6, Aladdin, China) was dissolved in deionized water and ultrasonicated for 10 min to obtain a 20% (w/v) P407 solution.[20,21] The solution was stored at 4°C until fully dissolved. The met-CDs were thoroughly dissolved in P407 solution and stirred gently for 30 min to prepare the thermosensitive hydrogel.

Rheological Analysis

The temperature-dependent sol-gel transition of the hydrogel was characterized by oscillatory rheology. Measurements were performed on a rotational rheometer (MCR302, Anton Paar, Austria) using a parallel plate geometry. Temperature sweeps were conducted from 10 °C to 40 °C at a heating rate of 3 °C/min. The experiment was carried out in oscillatory mode at a fixed frequency of 1 Hz and a constant strain of 1%. The evolution of the storage modulus (G') was monitored. All measurements were performed in triplicate on independently prepared batches.

In vitro Release Profile

The in vitro release behavior of Met-CDs from the hydrogel was evaluated by immersing a defined amount of hydrogel in phosphate-buffered saline (PBS, pH 7.4) and soaking it at 37 °C under gentle agitation (50 rpm) using a magnetic stirrer. At predetermined time intervals (0, 5, 10, 30, 60, and 120 min), aliquots of the release medium were withdrawn and replaced with an equal volume of fresh pre-warmed PBS to maintain sink conditions. The concentration of released Met-CDs was quantified using UV–Vis spectrophotometry (Biomate 3S, Thermo Scientific, USA) over the wavelength range of 200–400 nm.

Swelling Index

The swelling behavior of the hydrogel was assessed using a buoyancy-based gravimetric method. A beaker containing PBS preheated to 37 °C was placed on an analytical balance and tared. A piece of aluminum foil holding 3 mL of hydrogel was suspended in the solution using an external polyamides thread, ensuring full immersion and positional stability. Owing to its thermosensitive properties, the hydrogel adhered to the foil and remained stationary. The initial balance reading, corresponding to the upward buoyant force, was recorded as the baseline volume (V_0). Measurements were subsequently taken at 30, 60, 90, and 120 minutes. Volume expansion of the hydrogel over time was reflected by incremental changes in buoyant force, enabling quantitative evaluation of its swelling profile. The swelling index (*SI*) was calculated using the following equation:

$$SI = 100\% \times (V_t - V_0) / V_0$$

where V_0 represents the initial volume of the hydrogel, and V_t represents the volume at each time point. This index reflects the relative volume expansion of the hydrogel over time.

Agar Well Antibacterial Assay

The antibacterial activity of the Met-CDs@P407 hydrogel was further evaluated using an agar well antibacterial assay. Briefly, bacterial suspensions of *S. sanguinis, P. gingivalis*, and *F. nucleatum* were evenly spread onto the corresponding agar culture plates. Circular wells (3 mm in diameter) were then created in the agar plates. Three experimental groups were prepared: P407 hydrogel alone, free Met-CDs at the MBC for each bacterial species, and Met-CDs@P407 hydrogel containing the same concentration of Met-CDs. Equal volumes of each formulation were added into the wells and incubated under the corresponding culture conditions at 37 °C for 48 h. Antibacterial activity was evaluated based on the presence of bacterial growth inhibition surrounding the wells.

Establishment and Treatment of the Experimental Periodontitis Model

All animal experimental protocols were approved by the Ethics Committee of the 920th Hospital of Joint Logistics Support Force of PLA (Affiliated Joint Logistics Key Discipline Laboratory) (Approval No.: 2023–024-01), and were conducted in accordance with the standards outlined in the "Guide for the Care and Use of Laboratory Animals" and the ARRIVE guidelines (Animal Research: Reporting of In Vivo Experiments), in compliance with the institutional requirements of the Joint Logistics Key Discipline Laboratory. 30 six-week-old male Sprague–Dawley rats (200 ± 20 g) were randomly divided into five groups (n = 6 per group): (1) control, (2) periodontitis model without treatment, (3) Met-CDs hydrogel, (4) Met hydrogel, and (5) minocycline ointment. The rats were anesthetized with 2% pentobarbital sodium (0.2 mL/100 g) via intraperitoneal injection. Periodontitis was induced on the right maxillary first molar according to Zhang et al[22] Following disease induction, animals in the treatment groups received local administration of Met-CDs hydrogel, Met hydrogel, or minocycline ointment into the periodontal pockets once daily for four consecutive weeks, whereas the control and untreated periodontitis model groups received no intervention.

Hematological and Serum Biochemical Analysis

At the end of the 7-day treatment period, blood samples were collected under anesthesia to evaluate the short-term systemic response induced by the materials. Whole blood samples were subjected to routine hematological analysis using an automated veterinary hematology analyzer (BC-5000Vet, Mindray, China), including white blood cell (WBC), red blood cell (RBC), and platelet (PLT)-related parameters. Serum samples were obtained by centrifugation for biochemical analysis of liver and kidney function indicators using an automated biochemical analyzer (Dimension EXL200, Siemens, Germany), including alanine aminotransferase (ALT), aspartate aminotransferase (AST), and blood urea nitrogen (BUN)-related parameters. All analyses were performed according to standard laboratory procedures.

In vivo Systemic Inflammatory Response Evaluation

To evaluate the potential systemic inflammatory response induced by the materials, SD rats were randomly divided into four groups: blank control group (saline), commercial minocycline gel group, Met-CDs group, and Met-CDs@P407 group. The animals were administered the corresponding formulations by oral gavage once daily (1 mL per rat) for 7 consecutive days.

At the end of the treatment period, blood samples were collected under anesthesia, and serum was obtained by centrifugation. Serum levels of IL-6, IL-1β, and TNF-α were quantified using ELISA kits (IL-6, Cat# ERC003; IL-1β, Cat# ERC007; TNF-α, Cat# ERCa; NEOBIOSCIENCE, China) according to the manufacturers' instructions. Absorbance was measured using a microplate reader, and cytokine concentrations were calculated based on standard curves.

Bacterial Load Analysis

Bacterial load in the periodontal pockets was evaluated to assess the in vivo antibacterial efficacy of the treatments.[23] At designated time points (baseline, day 3, and day 7), subgingival samples were collected from the left maxillary first molar under anesthesia. Briefly, three sterile absorbent paper points (#40) were inserted into three equidistant sites within the gingival sulcus for 20s. The paper points were then transferred into sterile microtubes containing 1 mL of phosphate-buffered saline (PBS) and vortexed for 15 min to elute the bacteria.

Serial tenfold dilutions (up to 10^{-3}) of the bacterial suspensions were prepared. Aliquots (100 μL) from each dilution were spread onto BHI agar plates supplemented with blood and cultured under anaerobic conditions at 37 °C for 48 h. Colony-forming units (CFU) were counted, and the results were expressed as $\log_{10}$ (CFU mL^{-1}).

Imaging Analysis

After euthanasia, the right maxillary molars and alveolar bone were harvested. Microcomputed tomography (micro-CT) (NMC-100, PINGSENG Healthcare inc., China) was used to scan and reconstruct 3D images of the maxilla. The distance between the cementoenamel junction (CEJ) and alveolar bone crest (ABC) was measured at the mesial, distal, and central sites of the first molar, and the average distance was calculated to evaluate alveolar bone loss.

Systemic Toxicity Evaluation

The heart, liver, spleen, lungs, and kidneys were collected posttreatment and stained with hematoxylin and eosin (H&E) staining (G1120, Solarbio, China) to assess potential drug-induced organ damage. The harvested tissues were immediately fixed in 4% paraformaldehyde solution for 48 hours to preserve their morphological structure. Following fixation, the specimens were thoroughly washed, dehydrated through a graded ethanol series, cleared in xylene, and embedded in paraffin wax. Subsequently, the embedded tissues were sectioned into 4 μm thick slices using a rotary microtome. The tissue sections were mounted on glass slides, deparaffinized in xylene, and rehydrated through a descending series of ethanol concentrations to distilled water. The rehydrated sections were then stained with hematoxylin and eosin according to standard protocols. After staining, the sections were dehydrated again through an ascending ethanol series, cleared in xylene, and sealed with a neutral resin mounting medium.

Histological Staining and Immunofluorescence Analysis

Following Micro-CT scanning, the harvested maxillary bone specimens were fixed in 4% paraformaldehyde for 48 hours. The fixed specimens were then decalcified in EDTA solution (pH 7.4) until complete decalcification was achieved, as confirmed by a needle-prick test. Subsequently, the tissues were dehydrated through a graded ethanol series, cleared in xylene, and embedded in paraffin wax. Serial sections were cut at a thickness of 5 μm. To ensure unbiased sampling, every fifth section was systematically selected, yielding three representative sections per sample for subsequent staining procedures.

For histopathological evaluation, sections were stained with H&E to assess general tissue morphology and inflammatory infiltration. For immunohistochemistry, consecutive sections underwent antigen retrieval in citrate buffer (pH 6.0), peroxidase blocking, and incubation with primary antibodies against VEGF (ab32152, Abcam, UK) and TNF-α (AB_2913696, Thermo Fisher Scientific, USA) overnight at 4 °C. Signal development was performed using an HRP-conjugated secondary antibody (AB_2534782, Thermo Fisher Scientific, USA) followed by DAB chromogen staining, and sections were counterstained with hematoxylin. Stained slides were evaluated by blinded observers, and protein expression was semi-quantitatively analyzed based on staining intensity and the proportion of positively stained area.

Statistical Analysis

The data were analyzed via SPSS 27.0 software. Normality (Shapiro–Wilk test) and homogeneity of variance (modified Levene's test) were assessed before statistical analysis. One-way ANOVA or repeated-measures ANOVA was performed, with Holm–Sidak post hoc comparisons for intergroup significance. Statistical significance was set at $\alpha = 0.05$.

Results

Characterization of the Met-CDs

As shown in Figure 2A, the FTIR spectra revealed that Met functional groups were retained in the CDs synthesized at 180°C (CD-180), while those prepared at 250°C (CD-250) presented a greater degree of carbonization and fewer functional groups. Increasing the synthesis temperature led to an increase in the stretching vibration of the carboxyl and amide bonds, whereas the -NO_2 stretching vibration weakened (minimal changes in CD-180 but a significant reduction in CD-250). The bending vibrations of -CH_3 and -CH_2 decreased, the C-O stretching intensity decreased, and the =CH/-CH stretching vibrations increased (2900–3300 cm^{-1}). Additionally, at higher

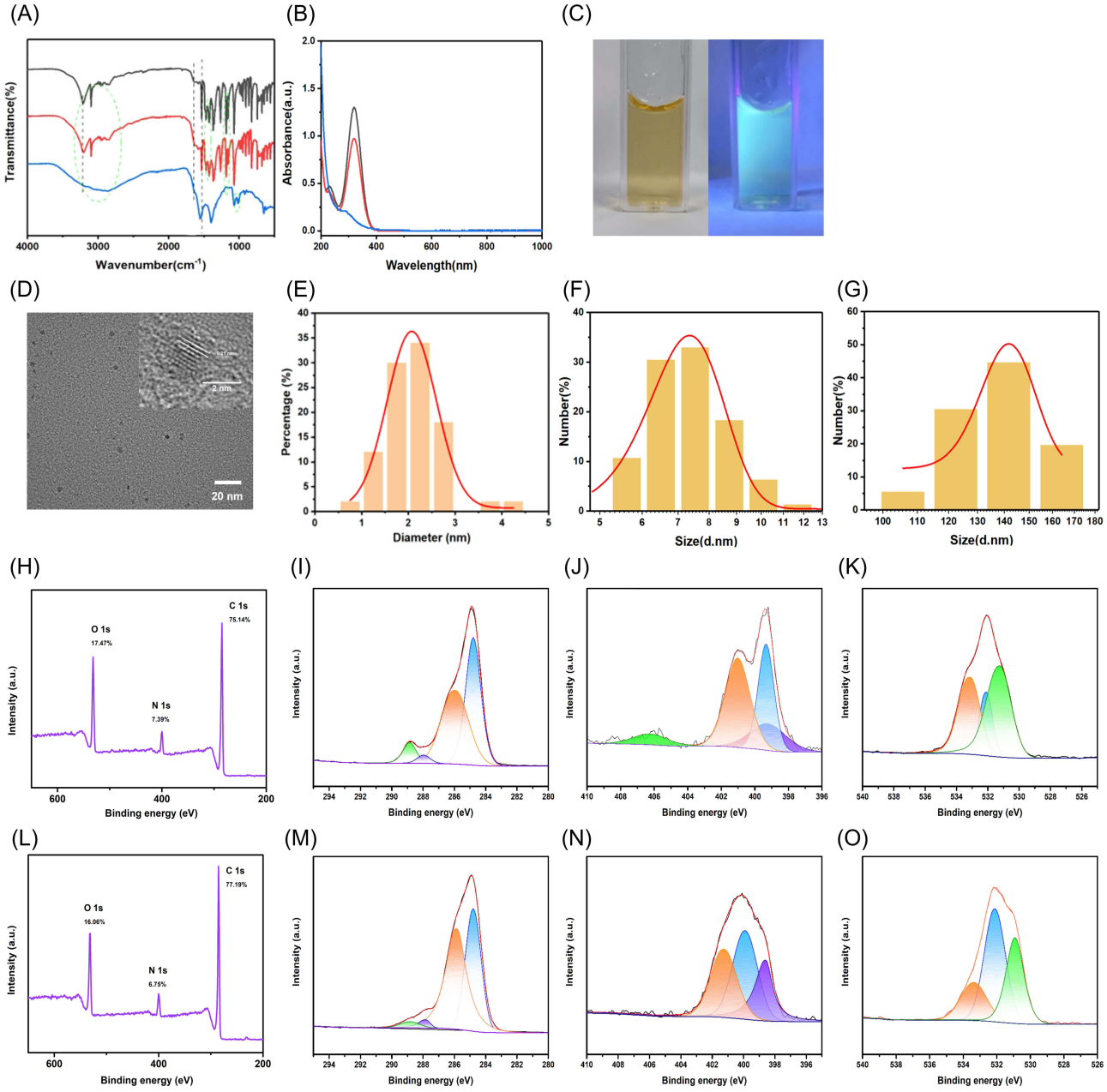

Figure 2 (**A**) FTIR spectra and (**B**) UV–Vis absorption spectra of Met (black), CD-180 (red), and CD-250 (blue). Green dashed circles indicate the locations of differential functional groups. (**C**) Optical images of sample CD-180 under ambient light and 365 nm UV illumination. (**D**) HRTEM image of CD-180 and (**E**) its particle size distribution. Hydrodynamic size distributions of CD-180 (**F**) and CD-250 (**G**) samples. XPS survey spectrum of CD-180 (**H**), and its high-resolution deconvoluted C 1s (**I**), N 1s (**J**) and O 1s (**K**) spectra. XPS survey spectrum of CD-250 (**L**) and its high-resolution deconvoluted C 1s (**M**), N 1s (**N**) and O 1s (**O**) spectra.

https://doi.org/10.2147/IJN.S604753

temperatures, some -NO_2 groups in the Met structure were reduced to -NH_2, and some -CH groups were oxidized to -COOH, which reacted with -NH_2 to form amide bonds (-CONH-).

The fluorescence spectra (Figure 2B) revealed that CD-180 exhibited two characteristic absorption peaks at 230 nm and 320 nm, similar to those of Met molecules. However, for the CDs synthesized at 250°C, the 230 nm absorption peak (π-π* transition) disappeared, while the 320 nm peak (n-π* transition) blueshifted and decreased in intensity. Under UV light irradiation, the CD-180 aqueous solutions displayed visible fluorescence (Figure 2C).

HRTEM images (Figure 2D) revealed that CD-180 was well dispersed and nearly spherical without significant aggregation, with a lattice spacing of 0.21 nm. CD-180 has a size range of 1.00–4.00 nm, with an average diameter of 2.07 nm (Figure 2E–F), whereas CD-250 ranges from 2.00–4.00 nm, with an average diameter of 2.90 nm.[14] With increasing synthesis temperature, the hydrated particle size of the CDs increased significantly, with that of CD-250 being approximately 20 times larger than that of CD-180 (Figure 2F–G).

The zeta potential of CD-180 was (−1.69±0.70) mV, whereas that of CD-250 was more negative (−8.11±0.30) mV. As the temperature increased, the zeta potential of both types of CDs gradually decreased.

XPS survey analysis (Figure 2H and L) showed that CD-180 contained slightly lower carbon but higher nitrogen and oxygen contents than CD-250, indicating a relatively more oxidized surface composition. High-resolution C 1s spectra (Figure 2I and M) revealed that both samples exhibited a dominant peak at ~284.6 eV corresponding to C–C/C=C bonds, suggesting similar carbon backbone structures. However, CD-180 displayed more pronounced features in the high binding energy region (~288–289 eV), which are associated with oxygen-containing groups such as C=O and O–C=O, indicating a higher degree of surface oxidation compared to CD-250. In the N 1s spectra, both samples showed main components within ~399–402 eV. Notably, CD-180 (Figure 2J) exhibited an additional distinct peak at ~405–406 eV, which can be assigned to oxidized nitrogen species, whereas this high-binding-energy component was not prominent in CD-250 (Figure 2N). Consistently, O 1s spectra indicated that CD-180 (Figure 2K) contained a broader distribution of high-binding-energy oxygen species (~533 eV), whereas CD-250 (Figure 2O) showed more concentrated peaks corresponding to C=O (~531 eV) and C–O (~532 eV), reflecting reduced oxidized functionalities.

Overall, these results suggest that the lower synthesis temperature favors the retention of polar and oxidized surface groups, whereas higher temperature promotes structural condensation. Based on these differences, CD-180 was selected for subsequent studies.

Cytotoxicity

Low cytotoxicity is essential for biomedical applications of CDs. HGFs were cultured in vitro, and a CCK-8 assay was used to evaluate cell viability following exposure to different concentrations of Met, Met-CDs and Met-CDs@P407 (16, 32, 64, 128, 256, 512, and 1024 μg/mL) for 24 h. Cell viability decreased with increasing drug concentration. At 1024 μg/mL, the Met-CDs maintained cell viability at 86.53%, while Met-CDs@P407 also exhibited a high viability of 83.67%, whereas the Met-treated cells showed a significantly lower viability of only 73.67%, indicating greater cytotoxicity than the Met-CDs did (Figure 3A).

To further evaluate drug-induced cell death, HGFs were incubated with different concentrations of the drugs for 24 h, stained with AM/PI dyes, and observed via fluorescence microscopy. Quantitative analysis of live/dead staining (Figure 3B) demonstrated a concentration-dependent decrease in HGF viability in all groups, with greater cytotoxicity observed in the Met group. Specifically, dead cells were detected in both the Met and Met-CDs@P407 group at 512 and 1024 μg/mL, the Met group showed live cell ratios of 97.05 ± 2.69% and 79.11 ± 1.02%, whereas the Met-CDs@P407 group exhibited 95.35 ± 0.70% and 90.89 ± 1.85% at the corresponding concentrations. In contrast, detectable cell death in the Met-CDs group was observed only at 1024 μg/mL, where the live cell ratio remained at 92.21 ± 2.25%. Representative fluorescence images (Figure 3C) were consistent with the quantitative results. Together with the CCK-8 data, these findings indicate that Met-CDs and Met-CDs@P407 exerted lower cytotoxicity toward HGFs than free Met, particularly at higher concentrations.

https://doi.org/10.2147/IJN.S604753

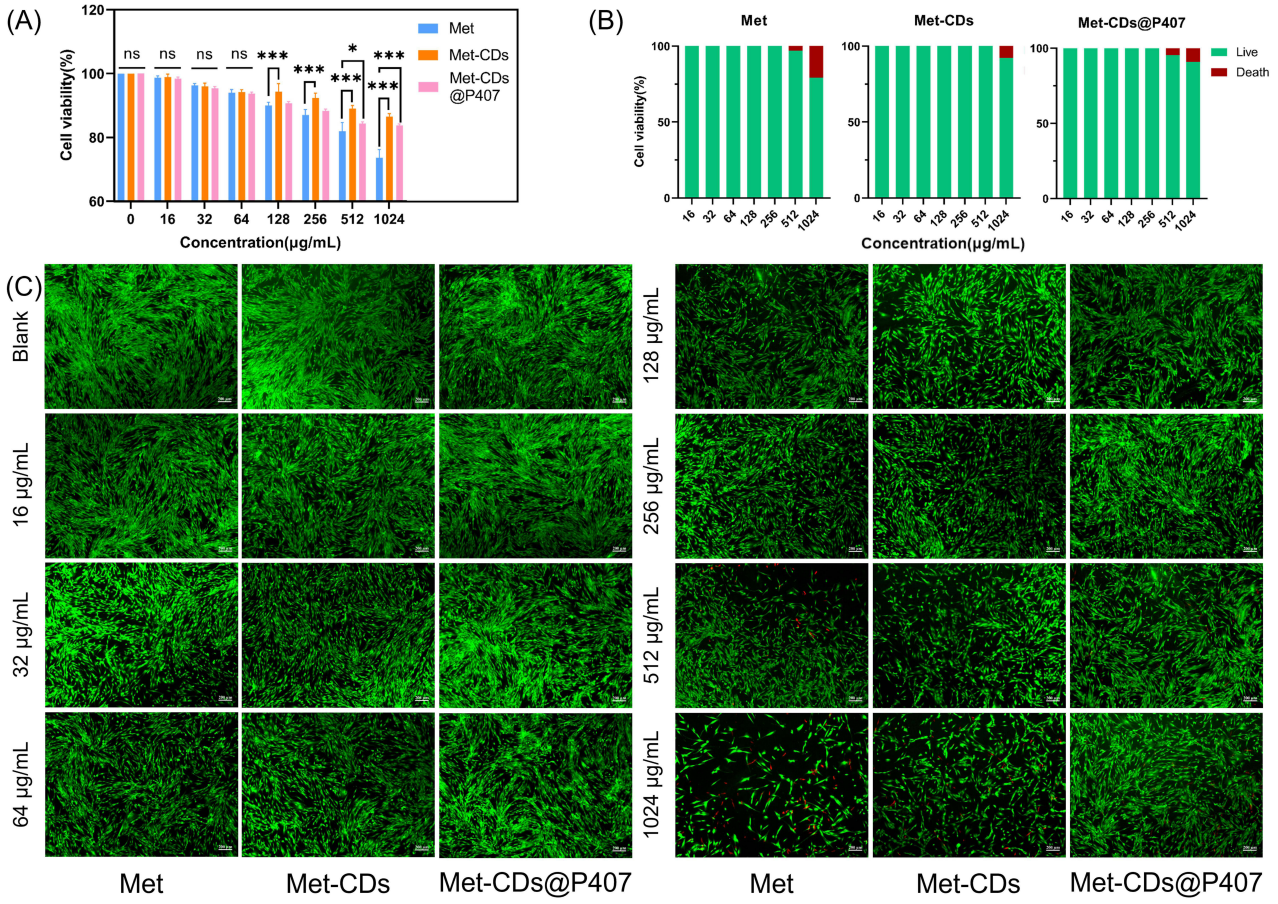

Figure 3 (**A**) CCK-8 cytotoxicity assay of cell viability after 24 h of exposure to different concentrations of Met, Met-CDs, and Met-CDs@P407. (**B**) Quantitative analysis of live/dead staining of HGFs after 24 h of treatment with different concentrations of Met, Met-CDs, and Met-CDs@P407. (**C**) Representative live/dead fluorescence images of HGFs after 24 h of incubation with Met, Met-CDs, and Met-CDs@P407 (scale bar = 200 μm). All groups were tested at concentrations of 16, 32, 64, 128, 256, 512, and 1024 μg/mL. (*$p < 0.05$, ***$p < 0.0001$).
Abbreviation: ns, not significant.

Antibacterial Properties of the Met-CDs

The antibacterial activity of the Met and Met-CDs was evaluated against the representative periodontal pathogens *S. sanguinis, P. gingivalis*, and *F. nucleatum* by determining their MIC and MBC values via the turbidity method. The results showed that *P. gingivalis* and *F. nucleatum* were highly sensitive to Met and the Met-CDs, with increased antibacterial activity observed upon CD incorporation. Table 1 indicates that the Met-CDs exhibited greater antibacterial efficacy against Gram-negative bacteria, particularly *F. nucleatum*, while higher concentrations were required for effective inhibition of Gram-positive bacteria.

Table 1 MIC and MBC Values of Met and Met-CDs Against *S. sanguinis* (*S.s.*), *P. gingivalis* (*P.g.*), and *F. nucleatum* (*F.n.*)

Bacterial Strain	Met	Met-CDs
	MIC/MBC (μg/mL)	MIC/MBC (μg/mL)
S. sanguinis (ATCC 10556)	1024/2048	256/512
P. gingivalis (ATCC 33277)	0.125/0.25	0.015/0.03
F. nucleatum (ATCC 25586)	0.03/0.06	0.0019/0.0038

Effects of the Met-CDs on Bacterial Metabolism

Bacterial metabolic activity was assessed by treating cultures with different concentrations of Met and Met-CDs via a CCK-8 assay. After 24 h, the results (Figure 4A–C) demonstrated that both the Met and the Met-CDs reduced the metabolic activity of *S. sanguinis, P. gingivalis*, and *F. nucleatum* in a concentration-dependent manner. However, the metabolic inhibition ability of the Met-CDs was significantly greater than that of Met at the same concentrations ($P<0.05$).

Live/dead bacterial staining results of *S. sanguinis* (Figure 4D), *P. gingivalis* (Figure 4E), and *F. nucleatum* (Figure 4F), observed by confocal laser scanning microscopy (CLSM), revealed that viable bacteria with intact membranes fluoresced green, while dead bacteria with damaged membranes fluoresced red. Correspondingly, semi-quantitative analysis based on the green/red fluorescence area ratio was performed, with the results presented at the bottom of the corresponding columns. Compared with that in the control group, bacterial mortality increased with increasing drug concentration. Notably, to achieve nearly 99.99% bacterial death under CLSM, the required Met-CDs concentrations were significantly lower than those of Met.

Disruption of Bacterial Biofilm Integrity and Cellular Structure by Met-CDs

SEM imaging (Figure 5A) was used to observe biofilm formation on the dentin surfaces following treatment with the Met and Met-CDs. In the control group, a dense biofilm was observed, with bacteria forming compact clusters. In both the Met and Met-CDs groups, the biofilm density decreased with increasing drug concentration, and the bacterial dispersion increased. At equivalent concentrations, the Met-CDs resulted in greater biofilm disruption than Met. These results suggest that compared with Met alone, Met-CDs more effectively damage bacterial outer membranes, reduce metabolic activity, induce bacterial death, and prevent biofilm formation.

To further investigate bacterial structural integrity, Western blot analysis was performed to assess the intracellular retention of GroEL, a highly conserved cytoplasmic protein, following treatment with Met and Met-CDs. As shown in Figure 5B, different retention patterns were observed among the three bacterial species. In *S. s*., no significant differences in GroEL expression were detected between the Met, Met-CDs, and blank groups, suggesting limited disruption of cellular integrity. In *P. g*., both treatment groups exhibited significantly reduced GroEL levels compared to the blank control, with the Met-CDs group showing a more pronounced reduction ($p = 0.002$) than the Met group ($p = 0.041$), indicating greater intracellular protein leakage and membrane damage. Similarly, in *F.* n., GroEL levels in the Met-CDs group were significantly lower than the blank control ($p = 0.002$), whereas the reduction observed in the Met group was not statistically significant. These findings further support that Met-CDs induce more extensive damage to bacterial membranes and cellular contents than metronidazole alone.

Characterization of the Thermosensitive and Physicochemical Properties of the Hydrogel

The thermosensitive behavior and physicochemical characteristics of the hydrogel were systematically evaluated, including sol–gel transition, rheology, in vitro release, and swelling performance.

The hydrogel was tested at two temperatures: room temperature (25 °C) and physiological temperature (37 °C, mimicking the periodontal pocket environment). As shown in Figure 6A, the hydrogel remained in a sol state at 25 °C, while a sol–gel transition occurred within approximately 5 minutes upon exposure to 37 °C. Corresponding rheological results are presented as a temperature–storage modulus curve in Figure 6B. Oscillatory rheology confirmed the thermosensitive gelation behavior, with a sharp increase in the storage modulus (G′) near 30 °C as temperature rose from 10 to 40 °C, indicating a rapid phase transition. G′ eventually plateaued at approximately 7000 Pa, suggesting the formation of a mechanically stable gel.

The in vitro release profile of the Met-CDs@P407 hydrogel is shown in Figure 6C. An initial burst release was observed within the first 10 minutes, followed by a sustained and gradual release phase. By 120 minutes, the cumulative release was nearly complete.

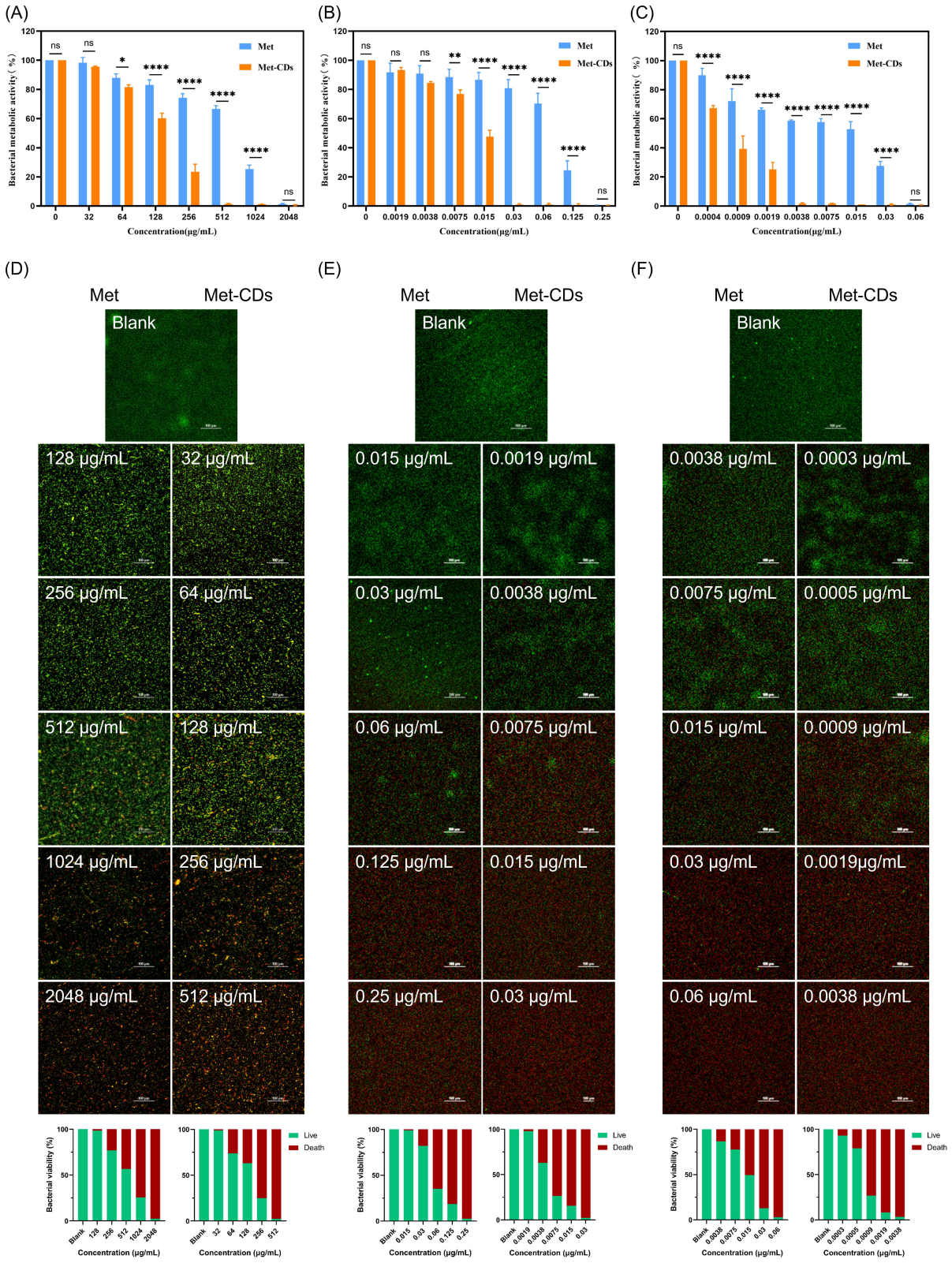

Figure 4 Effects of different concentrations of Met and Met-CDs on the metabolic activity of *S. sanguinis* (**A**) *P. gingivalis* (**B**) and *F. nucleatum* (**C**). Live/dead fluorescence staining of *S. sanguinis* (**D**) *P. gingivalis* (**E**) and *F. nucleatum* (**F**) after 24 h of coculture with Met and Met-CDs at different concentrations, as observed by CLSM (scale bar = 100 μm). Live bacteria are stained green, and dead bacteria are stained red. Semi-quantitative analysis based on the green/red fluorescence area ratio is presented below the corresponding images. (*p < 0.05, **p < 0.01, ****p < 0.0001).

Abbreviation: ns, not significant.

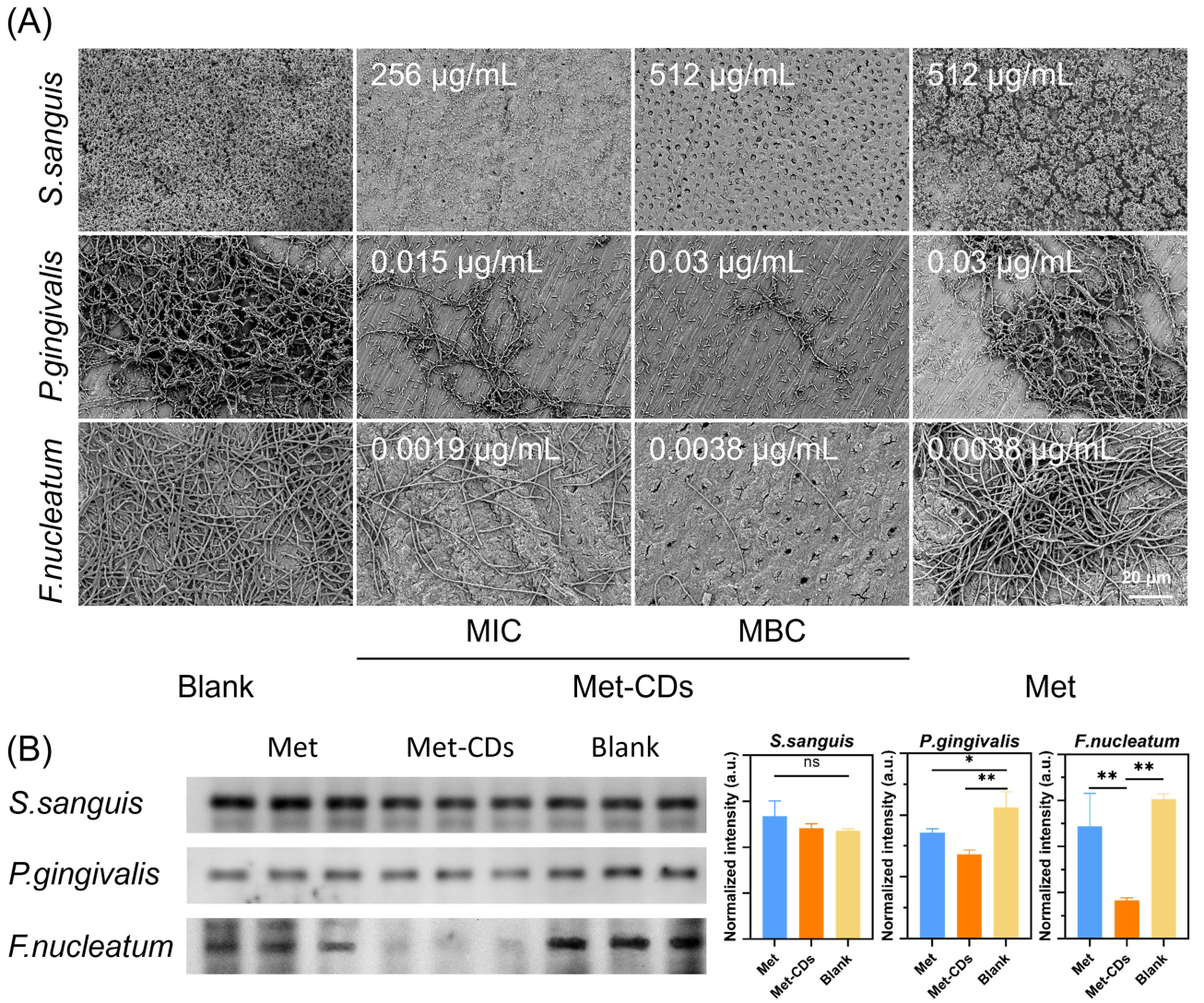

Figure 5 (**A**) SEM images showing the disruption of biofilm formation in three bacterial species treated with different concentrations of Met and Met-CDs (scale bar = 20 μm). (**B**) Western blot analysis of the intracellular protein GroEL in *S.s.*, *P.g.*, and *F.n.* following treatment with Met and Met-CDs at equivalent concentrations (equal to the MBC of Met-CDs for each strain). In *P.g.*, both treatment groups exhibited decreased GroEL retention compared to the blank control, with Met-CDs showing a more pronounced reduction. In *F.n.*, a significant reduction was observed only in the Met-CDs group. No significant differences were detected among groups in *S.s.* Protein loading was normalized using Ponceau S staining. (*p < 0.05, **p < 0.01).
Abbreviation: ns, not significant.

Swelling behavior is depicted in Figure 6D. The swelling index increased rapidly during the first 30 minutes, then gradually slowed, reaching approximately 5.5% at 120 minutes, after which the values tended to stabilize.

In vitro Antibacterial Evaluation of Met-CDs@P407 Hydrogel

The antibacterial activity of the Met-CDs@P407 hydrogel was further evaluated using an agar well antibacterial assay (Figure 6E). The P407 group showed no obvious bacterial growth inhibition against *S. sanguinis, P. gingivalis*, or *F. nucleatum*. For *S. sanguinis*, both the Met-CDs and Met-CDs@P407 groups exhibited visible inhibition regions with widths of approximately 2 mm. In *P. gingivalis*, elliptical inhibition regions were observed in both groups, with widths ranging from approximately 2–4 mm. Similarly, inhibition regions of approximately 2 mm were observed in the *F. nucleatum* groups.

https://doi.org/10.2147/IJN.S604753

https://doi.org/10.2147/IJN.S604753

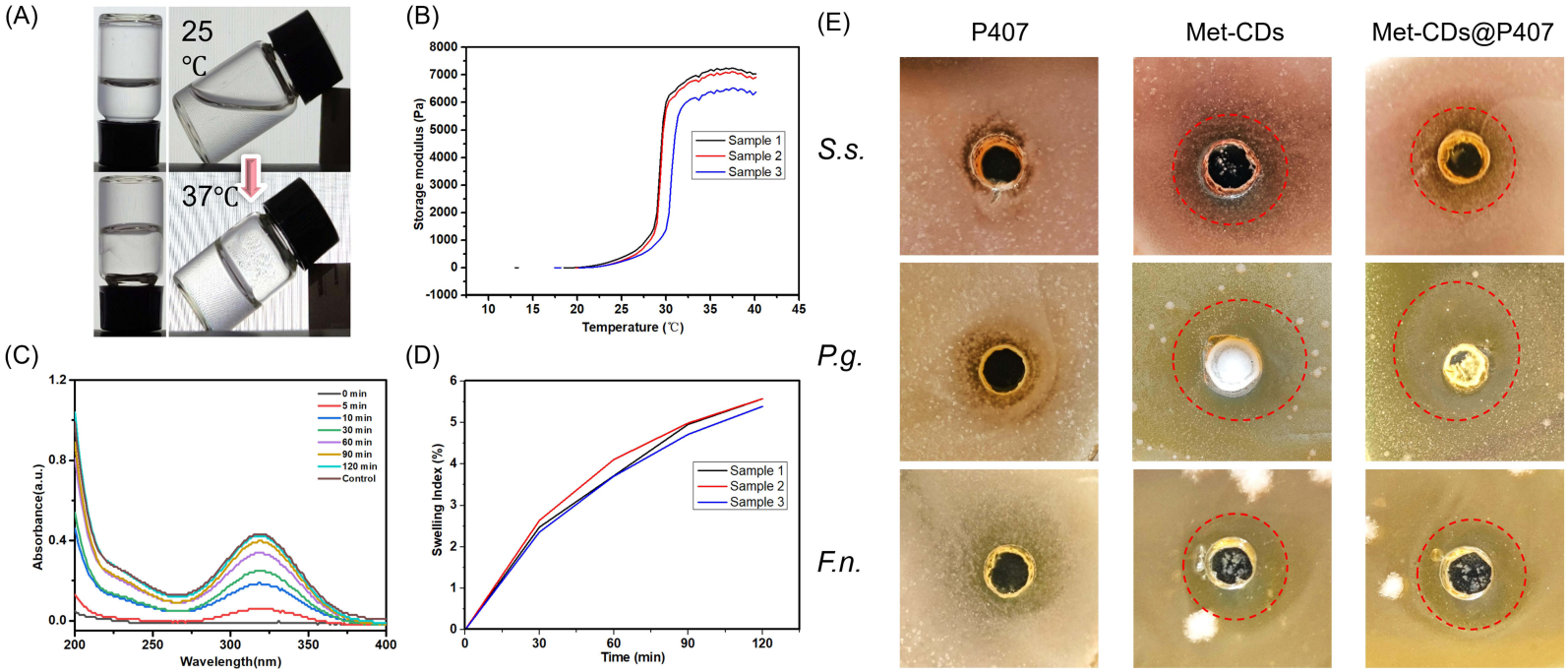

Figure 6 (**A**) Sol–gel transition of Met-CDs@P407 from the liquid state at room temperature (25°C) to the gel state at physiological temperature (37°C). The red arrow indicates the temperature transition process. (**B**) Temperature-dependent rheological profile, with a sharp increase in storage modulus (G′) near 30 °C, plateauing at ~7000 Pa. (**C**) In vitro cumulative release profile of Met-CDs from the hydrogel over 120 min. (**D**) Swelling index curve of the hydrogel within 120 minutes. (**E**) Agar well antibacterial assay of P407, Met-CDs, and Met-CDs@P407 against *S. sanguinis, P. gingivalis*, and *F. nucleatum*. Red dashed lines indicate the widths of the bacterial growth inhibition regions.

In vivo Biosafety Evaluation

To further evaluate the short-term systemic biosafety of the materials, routine hematological analysis, serum biochemical assays, and inflammatory cytokine ELISA were performed after 7 days of administration. The hematological and serum biochemical results showed generally stable blood and liver/kidney function parameters among the experimental groups. Although several individual parameters showed slight fluctuations, no obvious treatment-related abnormalities were observed overall (Supplementary Tables 1 and Supplementary Table 2). In addition, serum levels of IL-6, IL-1β, and TNF-α showed no obvious elevation in the Met-CDs@P407 group compared with the blank group (Figure 7A), indicating that the hydrogel system did not induce an apparent systemic inflammatory response under the tested conditions.

Following treatment, the in vivo biosafety of the Met-CDs thermosensitive hydrogel was evaluated. Gross anatomical examination performed at 4 weeks of major organs (heart, liver, spleen, lungs, and kidneys) showed normal morphology, color, and size, with no visible signs of congestion, edema, or hemorrhage. Histological analysis using hematoxylin and eosin (HE) staining (Figure 7B) further confirmed the absence of significant pathological abnormalities in all examined

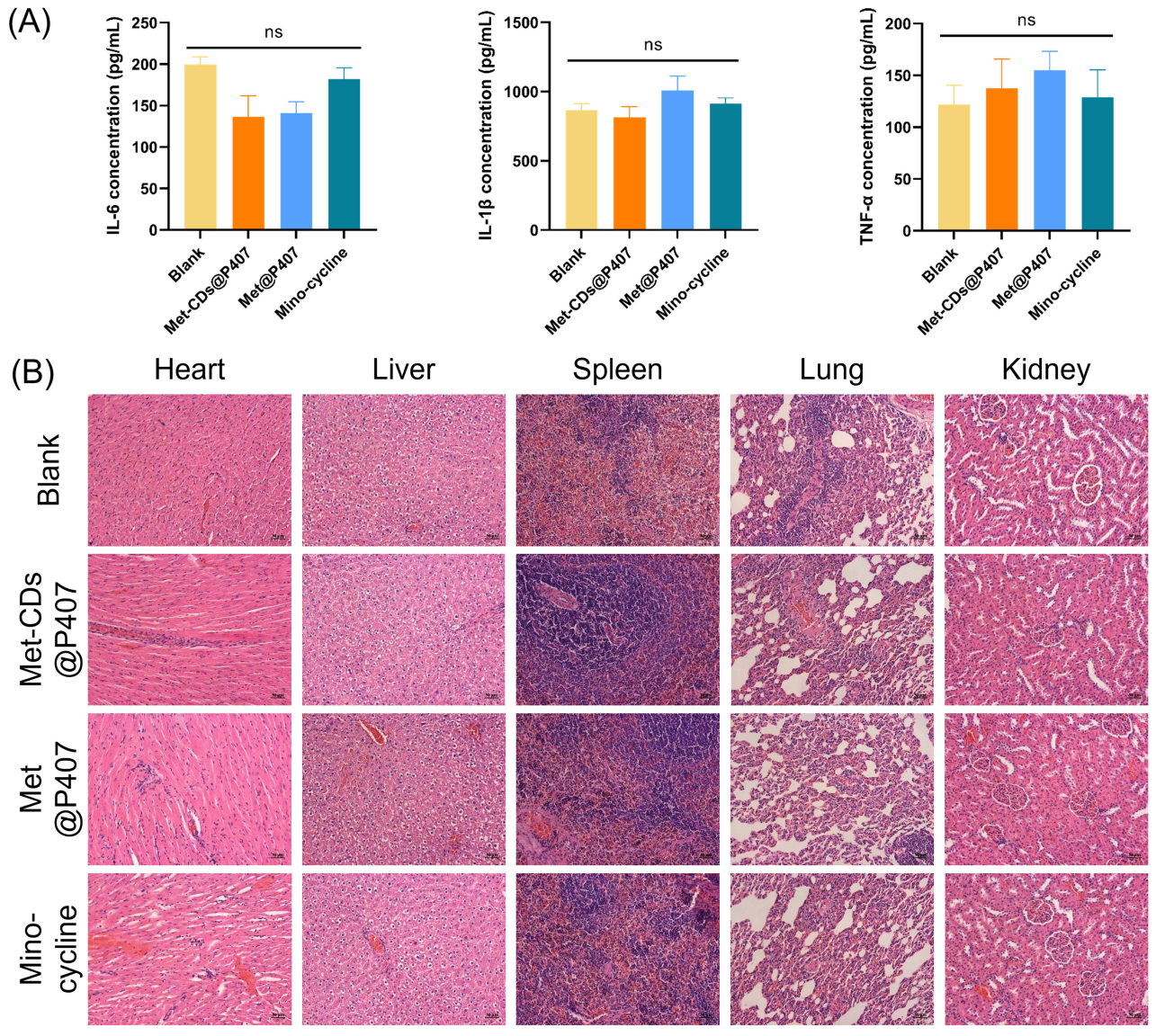

Figure 7 (**A**) Serum levels of IL-6, IL-1β, and TNF-α in SD rats after 7 days of oral administration of different formulations. (**B**) Histological analysis of major organs in SD rats following different drug treatments (scale = 50 μm).
Abbreviation: ns, not significant.

https://doi.org/10.2147/IJN.S604753

organs. These results indicate that the Met-CDs@P407 hydrogel exhibits good in vivo biocompatibility under the tested conditions.

In vivo Therapeutic Efficacy

An experimental periodontitis model was established in SD rats to evaluate the therapeutic efficacy of the Met-CDs thermosensitive hydrogel. Bacterial load in the periodontal pockets was quantified at different time points (Figure 8A). At baseline, no significant differences were observed among the groups. At day 3, all treatment groups showed reduced bacterial counts compared with the untreated model group, with a more pronounced reduction observed in the Met-CDs @P407 group. By day 7, the Met-CDs@P407 group exhibited the lowest bacterial load among all groups, indicating effective in vivo antibacterial activity.

Micro-CT analysis (Figure 8B) reconstructed three-dimensional images of the first molars in SD rats. Quantitative measurement of the cementoenamel junction to alveolar bone crest (CEJ–ABC) distance (Figure 8C) revealed significant alveolar bone resorption in the periodontitis group compared with the control group. Compared with the periodontitis and Met hydrogel groups, the Met-CDs hydrogel group presented significantly shorter CEJ-ABC distances ($P<0.05$), indicating effective inhibition of alveolar bone loss.

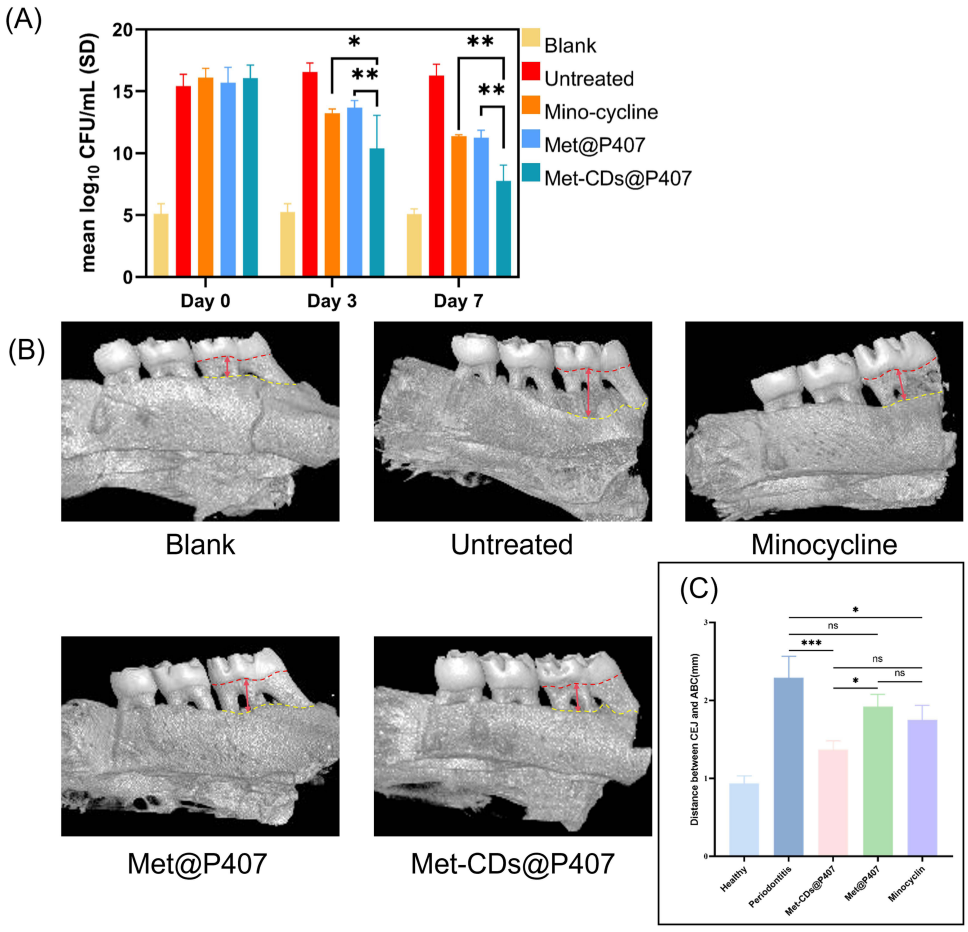

Figure 8 (**A**) Bacterial load in periodontal pockets of SD rats at different time points, expressed as $\log_{10}$ (CFU mL^{-1}). (**B**) Micro-CT reconstructed images of alveolar bone in SD rats. CEJ and ABC are indicated by red and yellow dashed lines, respectively, and the CEJ–ABC distance is marked with red arrows. (**C**) Quantitative analysis of the CEJ–ABC distance. (*p < 0.05, **p < 0.01, ***p < 0.001).
Abbreviation: ns, not significant.

Histological and Immunohistochemical Evaluation

Histological H&E staining of the periodontal tissues (Figure 9A) revealed an intact gingival epithelium with firm attachment to surrounding teeth in healthy control rats, with no inflammatory cell infiltration. In contrast, untreated periodontitis rats presented elongated epithelial rete ridges, dense inflammatory cell infiltration, and apical migration of the junctional epithelium, which are characteristic of inflammatory periodontal pathology. The Met hydrogel and minocycline groups showed mild reductions in inflammatory infiltration and rete ridge elongation, but apical migration of the junctional epithelium persisted. In the Met-CDs hydrogel-treated group, inflammation was markedly reduced, with minimal inflammatory cell infiltration, and the junctional epithelium appeared nearly normal, resembling that of healthy gingival tissue.

Immunohistochemical analysis was performed to evaluate the expression of vascular endothelial growth factor (VEGF) and tumor necrosis factor-α (TNF-α) in periodontal tissues. As shown in Figure 9B, VEGF staining exhibited low intensity across all groups. Although the untreated periodontitis group showed a slightly higher proportion of VEGF-positive areas, no statistically significant differences were observed among the experimental and control groups (Figure 9D). Meanwhile, TNF-α expression was significantly elevated in the untreated group compared to all other groups (Figure 9C). Quantitative analysis further demonstrated that all treatment groups exhibited significantly lower TNF-α expression levels than the untreated group ($p < 0.0001$), among which the Met-CDs@P407 hydrogel group showed the lowest TNF-α expression, approaching the level of the healthy control (Figure 9E). These findings indicate that the Met-CDs@P407 hydrogel effectively attenuates local inflammatory responses in periodontitis, while its effect on VEGF-mediated angiogenic activity remains limited.

These findings demonstrate that the Met-CDs@P407 thermosensitive hydrogel effectively inhibits periodontal pathogens, alleviates periodontal inflammation, and contributes to the preservation of periodontal tissue structure in an experimental periodontitis model.

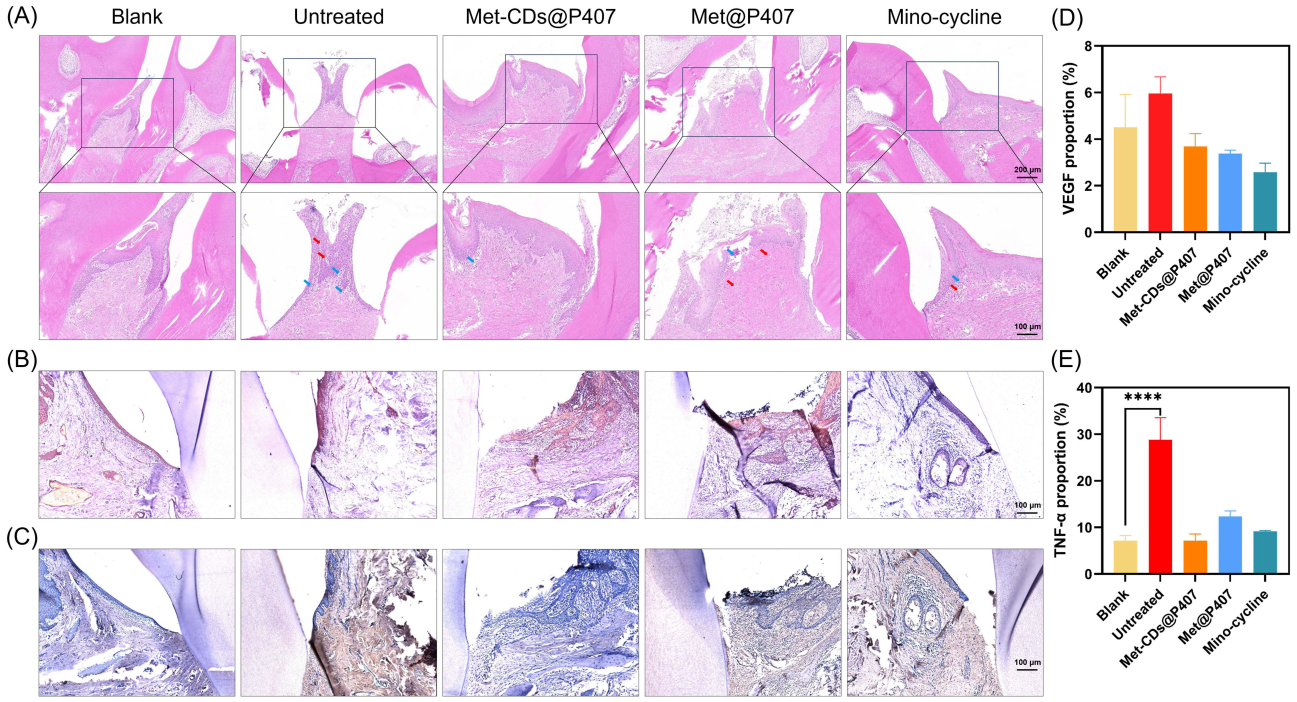

Figure 9 (**A**) H&E staining of gingival tissues surrounding the maxillary first molar in SD rats following different drug treatments. Red arrows denote mild vascular dilation, congestion, and hemorrhage; blue arrows highlight inflammatory cell infiltration. (**B**) Representative immunohistochemical staining images of VEGF in periodontal tissues from each group, showing weakly positive expression across all groups. (**C**) Representative immunohistochemical staining images of TNF-α in periodontal tissues from each group, with elevated TNF-α expression observed in the untreated periodontitis group (Scale bar = 100 μm). (**D**) Quantitative analysis of VEGF-positive staining area showed no statistically significant differences among groups ($p > 0.05$). (**E**) Quantification of TNF-α expression revealed significantly higher levels in the untreated group compared to other experimental and control groups (****$p < 0.0001$). The Met-CDs@P407 group exhibited a notably reduced TNF-α expression, comparable to the healthy control.

https://doi.org/10.2147/IJN.S604753

Discussion

Medication for periodontitis is essential for maintaining periodontal cleanliness, supporting scaling and root planing outcomes, and preventing disease progression.[24] However, conventional periodontal gel formulations face challenges due to saliva flushing and functional movements, leading to systemic drug absorption, reduced local retention, and the risk of toxicity and antimicrobial resistance.[8,25]

The antibacterial activity and potential cytotoxicity of metronidazole are attributed primarily to its nitro group and imidazole ring.[26,27] Under anaerobic conditions, the nitro group is reduced to form highly reactive intermediates, such as nitro anion radicals ($\cdot NO_2^-$) and nitroso compounds (R-NO), which contribute to its bactericidal effects.[28] The imidazole ring may interact with microbial enzyme systems, such as ferredoxin reductase, by acting as an electron transfer mediator to facilitate nitro group reduction and the generation of active intermediates.[29,30] Additionally, the lipophilicity of the imidazole ring enhances the ability of metronidazole to penetrate bacterial membranes and exert its antibacterial action intracellularly. However, resistant bacteria may evade the effects of metronidazole by reducing reductase activity or increasing drug efflux.[31]

In this study, compared with previously reported Met-CDs synthesized at 250 °C, Met-CDs prepared at 180 °C exhibited smaller particle sizes and a higher diversity and abundance of surface functional groups. This difference can be attributed to the temperature-dependent degree of carbonization during carbon dot formation. Specifically, high-resolution XPS deconvolution and FTIR analysis consistently indicated that Met-CDs synthesized at 180 °C preserved a higher proportion of hydroxyl and nitro-related groups, while carboxyl functionalities were newly introduced or markedly enriched, resulting in a more highly functionalized and hydrophilic surface. In contrast, increasing the synthesis temperature to 250 °C promoted more extensive decarboxylation, deoxygenation, and elimination of oxidized nitrogen species, leading to a higher carbonization degree. Concurrently, condensation and structural rearrangement occurred, driving the surface chemistry to evolve from highly oxidized moieties (eg., O–C=O and N–O species) toward more thermodynamically stable, moderately polar functionalities, such as C–O, C–N, and C=O bonds. This temperature-induced evolution of surface chemical states is likely a key factor underlying the observed differences in hydration behavior and hydrodynamic particle size between the two types of Met-CDs.[32] In antibacterial experiments, the Met-CDs demonstrated superior efficacy against *S. sanguinis, P. gingivalis*, and *F. nucleatum*, which are associated primarily with periodontitis. Compared with its precursor, metronidazole, Met-CDs require lower doses to achieve the same antibacterial effect while causing less cytotoxicity. Unlike metronidazole, carbon dots have a greater specific surface area, allowing more effective bacterial interactions.[33] Additionally, their ultrasmall size facilitates penetration through bacterial cell walls and erupts them, particularly the outer membrane of Gram-negative bacteria, enhancing their antibacterial efficiency.[34] This explains the observed differences in antibacterial effects between Gram-negative and Gram-positive bacteria in our research. Moreover, the introduction of $-NH_2$ groups on the carbon dot surface further contributed to its enhanced antibacterial properties.[35,36]

With respect to antimicrobial resistance, Met-CDs leverage their nanoscale advantages to counteract bacterial drug efflux pumps effectively.[37] Moreover, they may exert antibacterial effects via mechanisms partially distinct from metronidazole, potentially involving bacterial membrane disruption, which may be less dependent on conventional intracellular antibiotic targets.[38] This notion is further supported by our Western blot and SEM results, which revealed altered bacterial morphology, reduced biofilm integrity, and possible membrane-associated damage following Met-CDs treatment. However, it is noteworthy that Gram-positive bacteria (*S. sanguinis*) exhibited relatively lower susceptibility to membrane damage compared to Gram-negative species (*P. gingivalis* and *F. nucleatum*), which may contribute to the higher drug concentrations required for effective antibacterial activity. This observation may be related to the structural characteristics of Gram-positive cell envelopes, where the thicker peptidoglycan layer could partially limit the access of Met-CDs to the cytoplasmic membrane. In addition, even when membrane disruption occurs, the integrity of the cell wall may still influence the release of intracellular proteins, such as GroEL, which is consistent with the relatively higher protein retention observed in the bacterial pellets in the Western blot analysis. In addition, the negative surface charge of the Met-CDs reduces electrostatic repulsion with bacterial membranes, thereby enhancing biocompatibility and reducing

cytotoxicity.[39] Taken together, these attributes make the Met-CDs present an ideal antimicrobial material with improved efficacy and safety.

Furthermore, the thermosensitive properties of Poloxamer 407 enable the Met-CDs hydrogel to remain in a liquid state at room temperature and rapidly undergo sol–gel transition upon exposure to physiological temperatures within the periodontal pocket. This in situ gelation facilitates better spatial conformity to the irregular periodontal environment.[40] The in vivo efficacy of this delivery system in attenuating periodontal disease progression was substantiated in a rat model of experimental periodontitis. Further evidence from immunohistochemical analysis indicated that the Met-CDs @P407 hydrogel exerted a notable anti-inflammatory effect at the tissue level. While VEGF expression remained consistently low across all groups without statistical significance—indicating that the treatment exerted minimal influence on angiogenic activity, TNF-α levels were markedly reduced in the Met-CDs@P407 group compared with the untreated periodontitis group, with expression levels approaching those of the healthy control. These findings suggest that the hydrogel effectively suppresses local inflammatory responses, thereby contributing to the preservation of periodontal tissue.[41,42]

Although this study demonstrated that the Met-CDs@P407 hydrogel enhances antibacterial efficacy while reducing cytotoxicity, further research is needed to elucidate its precise mechanisms, such as potential photocatalytic effects or selective target activation. Additionally, the complexity of periodontitis in human populations warrants further clinical validation of its therapeutic efficacy.

Conclusion

In this study, metronidazole-derived carbon dots (Met-CDs) synthesized at a lower hydrothermal temperature retained relatively enriched polar and oxidized surface groups and exhibited enhanced antibacterial activity with lower cytotoxicity compared with metronidazole. Western blot analysis further suggested that the antibacterial effect of Met-CDs may be associated with bacterial membrane disruption. To improve local retention and clinical applicability in periodontal environments, a Poloxamer 407 (P407)-based thermosensitive hydrogel system was successfully constructed. The resulting Met-CDs@P407 hydrogel demonstrated favorable thermosensitive behavior, swelling properties, in vitro release characteristics, and retained antibacterial activity in vitro. In vivo studies further demonstrated that the hydrogel system possessed acceptable biosafety and effectively reduced periodontal bacterial burden and alveolar bone resorption in SD rats with experimental periodontitis. In addition, decreased TNF-α expression in periodontal tissues suggested that effective bacterial control by Met-CDs@P407 may contribute to the attenuation of local inflammatory responses. Collectively, these findings indicate that the Met-CDs@P407 thermosensitive hydrogel represents a promising localized antimicrobial biomaterial for adjunctive treatment of periodontitis and provides a potential strategy for improving periodontal antibacterial therapy through carbon dot-based nanomaterials.

Data Sharing Statement

The datasets used and/or analyzed during the current study are available from the corresponding author, Prof. Yuhong Xiao, upon reasonable request.

Ethics Approval and Consent to Participate

The experimental protocol was approved by the Ethics Committee of the 920 Hospital of the Joint Logistics Support Force of the Chinese People's Liberation Army (Number: 2023-024-01).

Author Contributions

All authors made a significant contribution to the work reported, whether that is in the conception, study design, execution, acquisition of data, analysis and interpretation, or in all these areas; took part in drafting, revising or critically reviewing the article; gave final approval of the version to be published; have agreed on the journal to which the article has been submitted; and agree to be accountable for all aspects of the work.

Funding

This work was supported by the National Natural Science Foundation of China (81970972), The Promoting Yunnan's Talent Support Program (XDYC-MY-2022-0053), and the Kunming Medical University First-Class Discipline Team Building Project (2024XKTDPY09).

Disclosure

A Chinese invention patent related to the materials reported in this study has been granted. The patent is titled "A Thermosensitive Hydrogel Comprising Metronidazole-Derived Carbon Dots, and Its Preparation Method and Applications" (Patent No. ZL 202410961282.5; Publication No. CN 118490628 B), and is assigned to the 920th Hospital of Joint Logistics Support Force of PLA. The inventors include several of the co-authors (Yuhong Xiao, Dingjie Wang, Xingrong Feng, Xiaodong Xing, Yuntong Hu), while the other author (Xiaoyi Tang) is not listed as inventors. The authors report no other conflicts of interest in this work.

References

1. Pihlstrom B, Michalowicz B, Johnson N. Periodontal diseases. *Lancet*. 2005;366:1809–1820. doi:10.1016/S0140-6736(05)67728-8
2. Tonetti MS, Greenwell H, Kornman KS. Staging and grading of periodontitis: framework and proposal of a new classification and case definition. *J Clin Periodontol*. 2018;45. doi:10.1111/jcpe.12945
3. Trindade D, Carvalho R, Machado V, Chambrone L, Mendes JJ, Botelho J. Prevalence of periodontitis in dentate people between 2011 and 2020: a systematic review and meta-analysis of epidemiological studies. *J Clin Periodontol*. 2023;50:604–626. doi:10.1111/jcpe.13769
4. Fayazi M, Rostami M, Moghaddam M, et al. A state-of-the-art review of the recent advances in drug delivery systems for different therapeutic agents in periodontitis. *J Drug Targeting*. 2024. doi:10.1080/1061186X.2024.2445051
5. Mugri MH. Efficacy of systemic amoxicillin–metronidazole in periodontitis patients with diabetes mellitus: a systematic review of randomized clinical trials. *Medicina*. 2022;58:1605. doi:10.3390/medicina58111605
6. Soares GMS, Figueiredo LC, Faveri M, Cortelli SC, Duarte PM, Feres M. Mechanisms of action of systemic antibiotics used in periodontal treatment and mechanisms of bacterial resistance to these drugs. *J Appl Oral Sci*. 2012;20:295–309. doi:10.1590/S1678-77572012000300002
7. Mombelli A, Edwards L, Nibali L. Empiric or individually targeted antimicrobial therapy. Historical perspective and current state. *Periodontology*. 2000;2025:rd.70008. doi:10.1111/prd.70008
8. Chen J, Dong S. Polymer-based antimicrobial strategies for periodontitis. *Front Pharmacol*. 2025;15:1533964. doi:10.3389/fphar.2024.1533964
9. Wang B, Booij-Vrieling HE, Bronkhorst EM, et al. Antimicrobial and anti-inflammatory thermo-reversible hydrogel for periodontal delivery. *Acta Biomater*. 2020;116:259–267. doi:10.1016/j.actbio.2020.09.018
10. Ali A, Saliem S, Abdulkareem A, Radhi H, Gul S. Evaluation of the efficacy of lycopene gel compared with minocycline hydrochloride microspheres as an adjunct to nonsurgical periodontal treatment: a randomised clinical trial. *J Dental Sci*. 2021;16:691–699. doi:10.1016/j.jds.2020.09.009
11. Pham DT, Phewchan P, Navesit K, Chokamonsirikun A, Khemwong T, Tiyaboonchai W. Development of metronidazole-loaded In situ thermo-sensitive hydrogel for periodontitis treatment. *Turkish J Pharmaceut Sci*. 2021;18:510–516. doi:10.4274/tjps.galenos.2020.09623
12. Fasiku Oluwaseun V, Omolo CA, Govender T. Free radical-releasing systems for targeting biofilms. *J Control Release*. 2020;322:248–273. doi:10.1016/j.jconrel.2020.03.031
13. Raza S, Ansari A, Siddiqui NN, Ibrahim F, Abro MI, Aman A. Biosynthesis of silver nanoparticles for the fabrication of non cytotoxic and antibacterial metallic polymer based nanocomposite system. *Sci Rep*. 2021;11:10500. doi:10.1038/s41598-021-90016-w
14. Goncalves S, Martins IC, Santos NC. Nanoparticle-peptide conjugates for bacterial detection and neutralization: potential applications in diagnostics and therapy. *Wiley Interdiscipl Rev Nanomed Nanobiotechnol*. 2022;14. doi:10.1002/wnan.1819
15. An Y, Wang Z, Wu F-G. Fluorescent carbon dots for discriminating cell types: a review. *Anal Bioanal Chem*. 2024;416:3945–3962. doi:10.1007/s00216-024-05328-3
16. Li P, Sun L, Xue S, et al. Recent advances of carbon dots as new antimicrobial agents. *SmartMat*. 2022;3:226–248. doi:10.1002/smm2.1131
17. Wang L, Pan H, Gu D, et al. A novel carbon dots/thermo-sensitive in situ gel for a composite ocular drug delivery system: characterization, ex-vivo imaging, and in vivo evaluation. *Int J Mol Sci*. 2021;22. doi:10.3390/ijms22189934
18. Liu J, Lu S, Tang Q, et al. One-step hydrothermal synthesis of photoluminescent carbon nanodots with selective antibacterial activity against porphyromonas gingivalis. *Nanoscale*. 2017;9:7135–7142. doi:10.1039/C7NR02128C
19. Kerner MJ, Naylor DJ, Ishihama Y, et al. Proteome-wide analysis of chaperonin-dependent protein folding in escherichia coli. *Cell*. 2005;122:209–220. doi:10.1016/j.cell.2005.05.028
20. Brambilla E, Locarno S, Gallo S, et al. Poloxamer-Based hydrogel as drug delivery system: how polymeric excipients influence the chemical-physical properties. *Polymers*. 2022;14. doi:10.3390/polym14173624
21. Chen Y, Lee J-H, Meng M, et al. An overview on thermosensitive oral gel based on poloxamer 407. *Materials*. 2021;14. doi:10.3390/ma14164522
22. Zhang X, Xu M, Xue Q, He Y. A modified method for constructing experimental rat periodontitis model. *Front Bioengineer Biotechnol*. 2023;10. doi:10.3389/fbioe.2022.1098015
23. Zhang J, Liang H, Zheng Y, et al. Photodynamic therapy versus systemic antibiotic for the treatment of periodontitis in a rat model. *J Periodontol*. 2019;90:798–807. doi:10.1002/JPER.18-0305
24. Jayachandran G, Thomas B, Karthika G. Rethinking therapeutics: drug repurposing in periodontal therapy: a narrative review. *J Clin Diagnostic Res*. 2024;18:ZE1–ZE6. doi:10.7860/JCDR/2024/71013.20138

25. Takallu S, Mirzaei E, Zakeri Bazmandeh A, Ghaderi Jafarbeigloo HR, Khorshidi H. Addressing antimicrobial properties in guided tissue/bone regeneration membrane: enhancing effectiveness in periodontitis treatment. *ACS Infect Dis*. 2024;10:779–807. doi:10.1021/acsinfecdis.3c00568
26. Upcroft J, Dunn L, Wright J, Benakli K, Upcroft P, Vanelle P. 5-Nitroimidazole drugs effective against metronidazole-resistant Trichomonas vaginalis and Giardia duodenalis. *Antimicrob Agents Chemother*. 2006;50:344–347. doi:10.1128/AAC.50.1.344-347.2006
27. Msa M, S J, K C. Systemic metronidazole in the treatment of periodontitis. *SunText Rev Dental Sci*. 2020;01. doi:10.51737/2766-4996.2020.024
28. Martinez-Gonzalez E, Frontana C. Inner reorganization limiting electron transfer controlled hydrogen bonding: intra- vs intermolecular effects. *Phys Chem Chem Phys*. 2014;16:8044–8050. doi:10.1039/c3cp55106g
29. Saxena A, Hegde V, Mutalikdesai S, Maste M. Versatility of Benzimidazole and ITS derivatives; An Insight. *J Pharmaceut Sci Res*. 2020;11:4152–4173. doi:10.13040/IJPSR.0975-8232.11(9).4152-73
30. Santra RC, Ganguly D, Singh J, Mukhopadhyay K, Das S. A study on the formation of the nitro radical anion by ornidazole and its significant decrease in a structurally characterized binuclear Cu(II)-complex: impact in biology. *Dalton Trans*. 2015;44:1992–2000. doi:10.1039/c4dt03362k
31. Nikaido H, Pagès J-M. Broad-specificity efflux pumps and their role in multidrug resistance of Gram-negative bacteria. *FEMS Microbiol Rev*. 2012;36:340–363. doi:10.1111/j.1574-6976.2011.00290.x
32. Sitnikova A, Gasilova E, Saprykina N. Carbon dots and carbon spheres produced by hydrothermal synthesis of oligochitosan solutions. In: 2024 International Conference on Electrical Engineering and Photonics (EExPolytech), IEEE, Saint Petersburg, Russian Federation, 2024:387–390. doi:10.1109/EExPolytech62224.2024.10755775.
33. Liang J, Li W, Chen J, et al. Antibacterial activity and synergetic mechanism of carbon dots against gram-positive and -negative bacteria. *ACS Appl Bio Material*. 2021;6937–6945. doi:10.1021/acsabm.1c00618
34. You Y, Yu X, Jiang J, et al. Bacterial cell wall-specific nanomedicine for the elimination of Staphylococcus aureus and Pseudomonas aeruginosa through electron-mechanical intervention. *Nat Commun*. 2025;16:2836. doi:10.1038/s41467-025-58061-5
35. Zarouki MA, Hejji L, Azzouz A, Aoulad El Hadj Ali Y, Muñoz AJ, Kailasa SK. Carbon nanostructures with antibacterial and wound healing activities: recent progress and challenges. *J Mater Chem B*. 2025;13:9745–9803. doi:10.1039/D5TB00272A
36. Santarelli G, Perini G, Salustri A, et al. Unraveling the potential of graphene quantum dots against Mycobacterium tuberculosis infection. *Front Microbiol*. 2024;15:1395815. doi:10.3389/fmicb.2024.1395815
37. Lei Z, Karim A. The challenges and applications of nanotechnology against bacterial resistance. *Vet Pharm Therapeut*. 2021;44:281–297. doi:10.1111/jvp.12936
38. Jia B, Du X, Wang W, et al. Nanophysical antimicrobial strategies: a rational deployment of nanomaterials and physical stimulations in combating bacterial infections. *Adv Sci*. 2022;9:2105252. doi:10.1002/advs.202105252
39. Yan J, Hou S, Yu Y, et al. The effect of surface charge on the cytotoxicity and uptake of carbon quantum dots in human umbilical cord derived mesenchymal stem cells. *Colloids Surfaces B Biointerfaces*. 2018;171:241–249. doi:10.1016/j.colsurfb.2018.07.034
40. Kerdmanee K, Phaechamud T, Limsitthichaikoon S. Thermoresponsive azithromycin-loaded niosome gel based on poloxamer 407 and hyaluronic interactions for periodontitis treatment. *Pharmaceutics*. 2022;14. doi:10.3390/pharmaceutics14102032
41. Afacan B, Keleş Yücel ZP, Paşali Ç, Atmaca Ilhan H, Köse T, Emingil G. Effect of non-surgical periodontal treatment on gingival crevicular fluid hypoxia inducible factor-1 alpha, vascular endothelial growth factor and tumor necrosis factor-alpha levels in generalized aggressive periodontitis patients. *J Periodontol*. 2020;91:1495–1502. doi:10.1002/JPER.19-0521
42. Karci B, Sokmen K. Changes in Gingival Crevicular Fluid Endocan (ESM-1) levels as a potential biomarker after non-surgical periodontal treatment in periodontitis patients. *Biomedicines*. 2025;13. doi:10.3390/biomedicines13051159